







Article

Detecting Water Hyacinth Infestation in Kuttanad, India, Using Dual-Pol Sentinel-1 SAR Imagery

Morgan David Simpson ^{1,*} , Vahid Akbari ², Armando Marino ¹, G. Nagendra Prabhu ³ , Deepayan Bhowmik ² , Srikanth Rupavatharam ⁴ , Aviraj Datta ⁴, Adam Kleczkowski ⁵, J. Alice R. P. Sujeetha ⁶, Girish Gunjotikar Anantrao ⁶, Vidhu Kampurath Poduvattil ⁶ , Saurav Kumar ⁷, Savitri Maharaj ² , and Peter D. Hunter ¹

- ¹ Faculty of Natural Sciences, University of Stirling, Stirling FK9 4LA, UK; armando.marino@stir.ac.uk (A.M.); p.d.hunter@stir.ac.uk (P.D.H.)
- ² Department of Computing Science and Mathematics, University of Stirling, Stirling FK9 4LA, UK; vahid.akbari@stir.ac.uk (V.A.); deepayan.bhowmik@stir.ac.uk (D.B.); savitri.maharaj@stir.ac.uk (S.M.)
- ³ Centre for Research on Aquatic Resources, Sanatana Dharma College, University of Kerala, Alleppey 688011, India; prabhugn@sdcollege.in
- ⁴ International Crops Research Institute for the Semi-Arid Tropics, Hyderabad 500007, India; r.srikanth@cgiar.org (S.R.); a.datta@cgiar.org (A.D.)
- ⁵ Mathematics and Statistics, University of Strathclyde, Glasgow G1 1XQ, UK; a.kleczkowski@strath.ac.uk
- ⁶ National Institute of Plant Health Management, Hyderabad 500030, India; dirpqniphm-ap@nic.in (J.A.R.P.S.); girish.ag@gov.in (G.G.A.); kpvidhu@gmail.com (V.K.P.)
- ⁷ Central Scientific Instruments Organisation, Chandigarh 160030, India; sauravpandey@csio.res.in
- * Correspondence: m.d.simpson@stir.ac.uk



Citation: Simpson, M.D.; Akbari, V.; Marino, A.; Prabhu, G.N.; Bhowmik, D.; Rupavatharam, S.; Datta, A.; Kleczkowski, A.; Sujeetha, J.A.R.P.; Anantrao, G.G.; et al. Detecting Water Hyacinth Infestation in Kuttanad, India, Using Dual-Pol Sentinel-1 SAR Imagery. *Remote Sens.* **2022**, *14*, 2845. <https://doi.org/10.3390/rs14122845>

Academic Editor: Sandra Eckert

Received: 29 April 2022

Accepted: 13 June 2022

Published: 14 June 2022

Publisher's Note: MDPI stays neutral with regard to jurisdictional claims in published maps and institutional affiliations.



Copyright: © 2022 by the authors. Licensee MDPI, Basel, Switzerland. This article is an open access article distributed under the terms and conditions of the Creative Commons Attribution (CC BY) license (<https://creativecommons.org/licenses/by/4.0/>).

Abstract: Water hyacinth (*Pontederia crassipes*, also known as *Eichhornia crassipes*) is a highly invasive aquatic macrophyte species, indigenous to Amazonia, Brazil and tropical South America. It was introduced to India in 1896 and has now become an environmental and social challenge throughout the country in community ponds, freshwater lakes, irrigation channels, rivers and most other surface waterbodies. Considering its large speed of propagation on the water surface under conducive conditions and the adverse impact the infesting weed has, constant monitoring is needed to aid civic bodies, governments and policy makers involved in remedial measures. The synoptic coverage provided by satellite imaging and other remote sensing practices make it convenient to find a solution using this type of data. While there is an established background for the practice of remote sensing in the detection of aquatic plants, the use of Synthetic Aperture Radar (SAR) has yet to be fully exploited in the detection of water hyacinth. This research focusses on detecting water hyacinth within Vembanad Lake, Kuttanad, India. Here, results show that the monitoring of water hyacinth has proven to be possible using Sentinel-1 SAR data. A quantitative analysis of detection performance is presented using traditional and state-of-the-art change detectors. Analysis of these more powerful detectors showed true positive detection ratings of ~95% with 0.1% false alarm, showing significantly greater positive detection ratings when compared to the more traditional detectors. We are therefore confident that water hyacinth can be monitored using SAR data provided the extent of the infestation is significantly larger than the resolution cell (bigger than a quarter of a hectare).

Keywords: water hyacinth; Sentinel-1; SAR; change detection

1. Introduction

India's waterways cater to a wide range of utilities, e.g., transport, energy generation, irrigation, ecosystem services, etc., as well as supplying drinking water. Inland waterways used to play an important role for freight movement and transportation in India for centuries; however, this has seen a steady decline since the introduction of railways in the nineteenth century and with the improvement of road infrastructure [1]. Increasing automobile density and vehicular pollution in urban clusters have reinvigorated interest

in inland water transport as a viable alternative or addition to rail and road-based transportation [2]. According to a report by Statista, about 41.49% of the workforce in India was employed in agriculture in 2020 [3]. Thus, it is not surprising that agricultural irrigation is the main use of these waterways; however, hydroelectric power generation, industrial sector demands and potable water supply are the other main water usages. As an effect of climate change, the traditional southwest and northeast monsoon patterns have become increasingly unpredictable over the last few decades. Unpredictable onset of monsoon, less uniform distribution of the rainfall over the traditional monsoon periods and frequent dry spells have enhanced the vulnerability of livelihoods dependant on rainfed agriculture. Thus, 67% of agriculture that is rainfed may have to look for supplementary sources of irrigation from surface waters to reduce their vulnerability to the vagaries of climate change [4].

Many lakes in India are under stress from multiple anthropogenic pressures, which has led to an increase in invasive species [5]. Water hyacinth (*Pontederia crassipes*) is an aquatic plant, indigenous to tropical South America and a highly invasive species [6]. It was introduced to India in 1896 [7] and now occurs in freshwater lakes, rivers, irrigation channels, streams and most other surface waters throughout the country. Water hyacinth was identified by the International Union for Conservation of Nature (IUCN) as one of the most dangerous invasive species in the world due to its capacity for growth and considerable socio-economic repercussions [8]. Water hyacinth is characterised by its reproductive capabilities, rapid dispersal and growth [9] due to its ability to cause the following major environmental and socio-economic problems: (i) a decrease in dissolved oxygen concentration in open waters, particularly during the non-photo periods, causing anoxic states and reducing fish populations [10]; (ii) damage to fishing boats and other inland water transportation, including increases in fuel consumption, boat repairs and a reduction in boat lifespan [11]; (iii) transport delays caused by blockages to canals, rivers and small channels [12]; (iv) reductions in water flow and damage/power loss to hydroelectric power stations [13], as well as blockages to agricultural irrigation [14]; (v) degradation and/or loss of drinking water, with potential health risks [15,16]; (vi) increases in disease vectors, such as mosquitoes, that are attracted to the plant habitat and reduced water flow [17,18].

The monitoring of aquatic plant infestations has traditionally been field-based measurements. However, this presents several challenges. Aquatic vegetation, like water hyacinth, are capable of covering large geographic areas. In tandem with this, water hyacinth can also block access to study sites through the density of the plant infesting waterways, causing major accessibility issues. The growth rate of invasive aquatic plants, especially water hyacinth, is typically high. Fast-flowing currents can also rapidly change the position of the free-floating plants and cause field-based measurements to be required on a highly temporal basis. Monsoon season in India is increasing in variability, causing timings for field-based measurements to change if seasonal monitoring is needed. Finally, encompassing all of these issues is the problem of budgeting. Due to the nature of field sampling, budgeting issues can arise from the high temporal and spatial coverage required to monitor the spread of aquatic plants. Therefore, data gaps may be introduced in areas where field sampling cannot be afforded.

Use of a multi-modal approach when monitoring water hyacinth is necessary to overcome the challenges listed above [19], and this work contributes towards the beginnings of a multi-modal approach via Synthetic Aperture Radar (SAR) remote sensing. Since SAR provides its own illumination and microwaves penetrate most weather conditions, the monitoring technique can image the study area under any weather condition and independent of day or night-time conditions. The spatial and temporal coverage provided by freely available SAR data, such as the European Space Agency's Sentinel Programme satellites, Sentinel-1A and Sentinel-1B, provide monitoring without accessibility issues and budget issues and are capable of monitoring changes in the growth of plants throughout the seasons.

2. Remote Sensing as a Means of Monitoring Aquatic Plants

2.1. Optical Systems

Due to its synoptic coverage, satellite imaging has been used extensively in monitoring water quality. Remotely sensed data, primarily through multispectral and hyperspectral optical satellite data reflectance spectra, have been widely used in the monitoring of surface waters. The use of band ratio-type algorithms measuring sediment load, chlorophyll-a, coloured dissolved organic matter (CDOM), pollutants and other qualitative parameters [20–22].

When it comes to monitoring macrophytes, Everitt et al. (1999) [23] could distinguish water hyacinth at multiple different study sites in colour infrared imagery across a temporal scale. Ground data were used to generate a computer classification of the study site; a subsequent confusion matrix indicated that water hyacinth had a producer and users accuracy of 84.6% and a kappa estimate of 0.828. Shilpakar et al. (2017) [24] used optical images captured from Landsat-8 to monitor potential water hyacinth infestations within the Gwydir Wetlands, Australia. However, due to the 30 m spatial resolution of Landsat-8, fine spatial accuracy is difficult to achieve. Therefore, provided that we have cloud-free images, the use of optical satellite was determined applicable for identifying potential weed infestations. An unsupervised classification of 83% when mapping and identifying plant species was achieved using Quickbird multispectral data in Turkey [25]. However, mixed pixels were recognised as a main limitation in the monitoring process. Sun et al. (2021) [26] used Sentinel-2 time-series data to classify wetlands vegetation in flooded areas, where an overall accuracy of ~0.91 was obtained using the modified normalised difference water index (MNDWI).

An increase has recently been seen in the use of small drone aircraft and UAVs for the monitoring of aquatic environments. This includes wetlands [27], rivers [28], bogs [29] and lakes [30]. High-resolution drone aerial surveys were undertaken to monitor the Trent-Severn Waterway in Canada [31]. A collection of radiometrically calibrated multispectral drone imagery was classified using a supervised automated classification algorithm with a supervised machine-learning Random Forest classifier. Using this, Chabot et al. (2013) [31] found their classification algorithm to have an accuracy of 84% when classifying submerged vegetation and an overall accuracy of 92% when classifying above-surface aquatic vegetation. Lee et al. (2017) [32] found that the use of drone-based imagery could accurately identify the existence of aquatic plants in the Muncheon water reservoir, South Korea, when a Normalised Difference Vegetation Index (NDVI) and Surface Algal Bloom Index (SABI) were applied.

UAV data can be coupled with very high-resolution (VHR) satellite imagery to train Support Vector Machines in classifying estuarine environments. Gray et al. (2018) [33] used UAV data with WorldView-3 and RapidEye of the Rachel Carson Reserve, USA, with an SVM to examine change between 2004 and 2017. It was found that wetland vegetation mapping could be achieved with an accuracy of up to 96% when classifying the estuarine site, which is similar to those of previous studies that have achieved classification accuracies of 93% [33] and 95% [34].

2.2. Radar Systems

This work is mainly concerned at producing a monitoring methodology for early detection. Early detection of water hyacinth movement and regrowth has the potential to cut costs of removal and stunt the growth of the weed before it damages the environment. Due to cloud cover, optical systems struggle to provide useful images, particularly during the rainy season [35,36].

Previous studies using remotely sensed optical data have experienced data gaps in temporal acquisitions that range from weeks to months while monitoring surface waters and water hyacinth [37,38]. Ghoussein et al. (2019) [38] studied water hyacinth presence on the Al Kabir River using Sentinel-2 imagery: a full two months of data, January and February 2018, were unavailable for inspection due to cloudiness.

Therefore, it is paramount to understand if a system that can acquire data in any weather condition, such as SAR, can be used when optical data are not available.

SAR has been largely applied to water quality when it comes to detecting oil pollution [39]. The use of SAR in monitoring wetlands has also been demonstrated due to the ability to penetrate vegetation and provide information regarding vegetation structure and ground contribution [40]. Using SAR to distinguish between herbaceous vegetation forest and water within the Amazon Basin, Hess et al. (2015) [41] classified SAR mosaics. A producer's accuracy of 85% was achieved when classifying aquatic macrophytes, woody vegetation and wetland area. However, it is noted within the study that high confusion rates were seen in the backscattering signatures for shrub and aquatic macrophytes. Mohammadimanesh et al. (2017) [42] commented on how Interferometric SAR (InSAR) is a promising tool for monitoring wetland water bodies, with detailed quantitative maps of vegetation and water level variations providing valuable information. However, while the use of InSAR has great potential, there are still limitations associated with interferometric coherence, phase discontinuity and a dependency on ground-based hydrological observations to calibrate and validate InSAR observations [42,43].

2.3. Combined Use of Systems

Finally, the use of radar and optical data by image fusion techniques can also be used, which can allow for better mapping and discriminative results [44]. Land-cover maps using image fusion techniques using Radarsat-1 and Landsat TM have been used to allow for the species-level discrimination of macrophyte stands [45]. Cavalli et al. (2009) [46] monitored Lake Victoria using a mixture of optical and radar techniques through ENVISAT, ASTER and Landsat data. The study applied a classification algorithm to ETM+ data derived from Landsat, allowing for the discrimination of water hyacinth, as the main aquatic vegetation species, as well as Nile cabbage, water lily, hippo grass, papyrus, water fern, reeds and *Typha* sp. present within the lake. It was also found that, using a combination of ASTER and ENVISAT, a time-series of the weed proliferation was produced; however, the time series data of weed proliferation in the years 2005 and 2006 were deemed highly variable.

In this work, we address the following research questions:

1. Is water hyacinth within Vembanad Lake visible in SAR imaging?
2. Can the use of change detectors be implemented to monitor water hyacinth within Vembanad Lake?

The novelty of this paper is that for the first time, we show that SAR can obtain high level accuracy of detections for water hyacinth on Vembanad Lake, Kuttanad, India. We show that using Single Look Complex (SLC) data also improves the detection performance when compared with simple thresholding of Ground Range Detected (GRD) data, with SLC data capable of reaching accuracies as high as 98% with 0.1% false alarm rates when using powerful change detection methods. Finally, for the first time, we produce a heatmap showing the water hyacinth presence/coverage over a 2-year time-frame, which can be used to aid management practices within the area.

3. Methodology and Materials

3.1. Study Area

Kuttanad, Kerala is a paddy-rich region in southwest India. The region covers 875 km² with wetlands comprising more than two-thirds of the land area. The department of agriculture has reported that pesticide usage of farmers in the Kuttanad region is twice as high as usage found within the other states, and that the waters are rich in pesticides and fertilisers [12]. This has resulted in an increase in water hyacinth found within the major lakes of the region. Impacts have been felt on drinking water, fisheries, transport, irrigation and recreational use of the water bodies due to the presence of water hyacinth within the region's waterways. This study focusses on the largest Ramsar site in Kerala, Vembanad Lake.

3.2. Satellite Data

Courtesy of the European Space Agency (ESA) Copernicus programme, dual-polarimetric Sentinel-1 SAR data were obtained. The mode of acquisition is Interferometric Wide Swath (IW), Ground Range Detected (GRD) and Interferometric Wide Swath Single Look Complex (SLC). The spatial resolution of the SAR images is approximately 20×20 m (for GRD) or 20×5 (for SLC) with a temporal resolution of up to 6 days on Vembanad Lake (12 days using a single orbit). A total of 46 images were acquired from January 2019–January 2021, consisting of 11 GRD acquisitions for single image analysis and 46 SLC acquisitions for change detection analysis.

3.3. SAR Pre-Processing

GRD products consist of SAR data that have been calibrated (sigma naught), multi-looked and projected to ground range using an Earth ellipsoid model, where the resulting product has reduced speckle. SLC products are represented by complex numbers (I and Q) and contain information on both amplitude and phase of the electromagnetic wave. In this research, we considered the information in polarimetric data as well. We evaluated the elements of the polarimetric covariance matrix, which include intensity of co-polarisation (VV) and cross-polarisation channels (VH) and their cross-correlation (VV*VH). Where V stands for vertical linear, and H stands for horizontal linear.

3.4. Scattering Model for Water Hyacinth

Water hyacinth will increase the surface roughness of the lake surface and will therefore introduce a difference in backscattering in the image, as seen in Figure 1.



Figure 1. Scattering mechanisms present from radar satellite within a water hyacinth infested canal.

Model for clean water surface: A calm, clean water surface will cause the electromagnetic wave to bounce in a specular direction. This will make clean areas of the lake appear dark, as the majority of the microwave signal is scattered away from the sensor.

Model for water hyacinth surface: A rougher surface on top of the lake, such as a mat of water hyacinth, will cause the signal to scatter in different directions. This volumetric scattering will be prominent in areas of water hyacinth infestation as the radar signal hits multiple hyacinth leaves before exiting the vegetation and volumetrically scattering towards the sensor.

If we assume the targets are spatially separated, we can represent the backscattering as:

$$I_b = I_w(\sigma_w) + I_h(\sigma_h, \epsilon_h) + I_d(\sigma_w, \sigma_h, \epsilon_h) \quad (1)$$

where I_b is backscatter, I_w is the scattering from water, I_h is scattering from the plant and I_d is double reflection. σ_h is the roughness of the hyacinth and σ_w is the roughness of the water. Finally, ϵ_h and ϵ_w are the dielectric constant of hyacinth and water, respectively. The smoother the water is, the smaller I_w will be, and I_d will be higher. The greener and thicker the plant is, the higher the I_h value will be.

Differences in backscattering values between clean water and water hyacinth will make discrimination of both targets capable as shown in Figure 1.

3.5. Water Hyacinth Detectors

We can start setting the detection task as one to separate a pixel in two classes. The first class, defined “clean”, represents pixels of lake that are not infested by water hyacinth. The second class, defined “infested”, includes the presence of water hyacinth.

We pursued two separate frameworks for detecting water hyacinth in lakes:

1. In the first, we use a single image of the lake, and we try to separate the pixels of clean and infested using statistical differences between the VV and VH intensity images. The advantage of this method is the simplicity and computational efficiency.
2. In the second, we take advantage of Sentinel-1 multitemporal images to apply a change detector to identify when water hyacinth has started growing in the lake. The advantage of this method is the fact that it benchmarks the pixel value and therefore is expected to be more robust against noise and the eventual variability of water pixels.

3.6. Single Image Detection Using Statistical Analysis

Sentinel-1 GRD images were processed (Figure 2) to determine if water hyacinth could be seen in SAR images of the Vembanad Lake. As shown in Figures 3 and 4 (described in the next section) we can clearly observe areas where the backscattering of the lake is significantly higher.

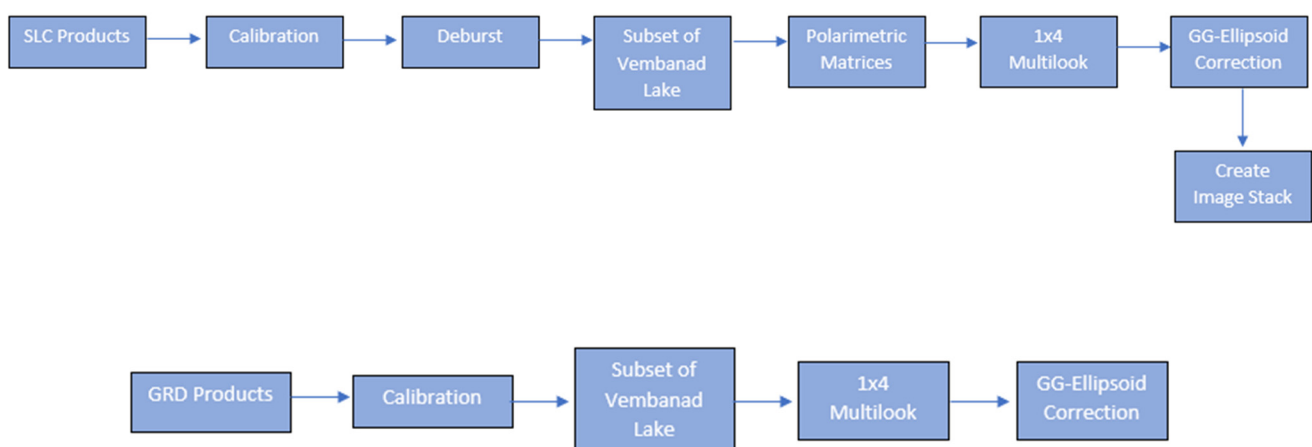
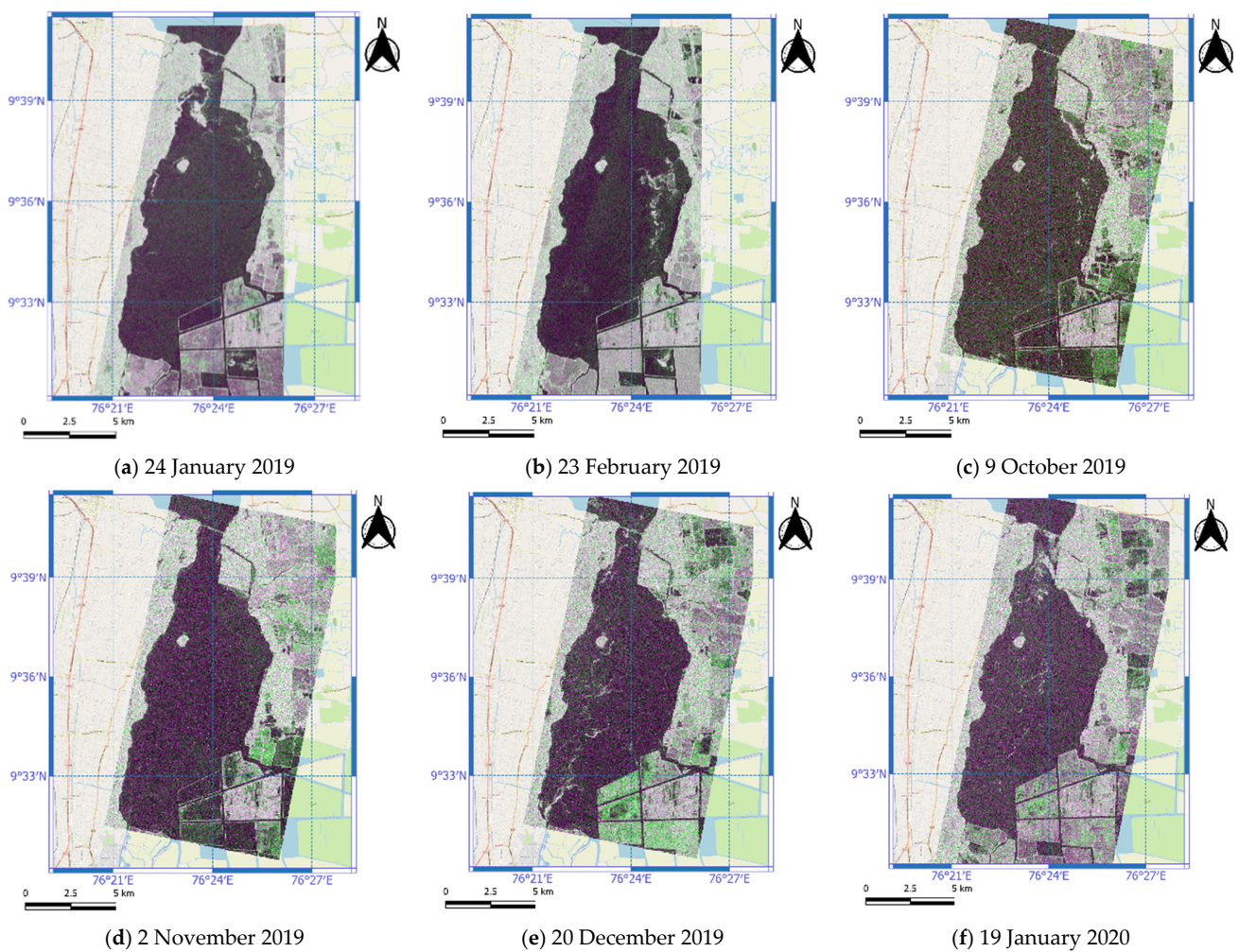


Figure 2. Flow chart showing methods used in SLC and GRD data processing.



Figure 3. Water hyacinth infestation in Vembanad Lake, India. Image taken 26 January 2020.



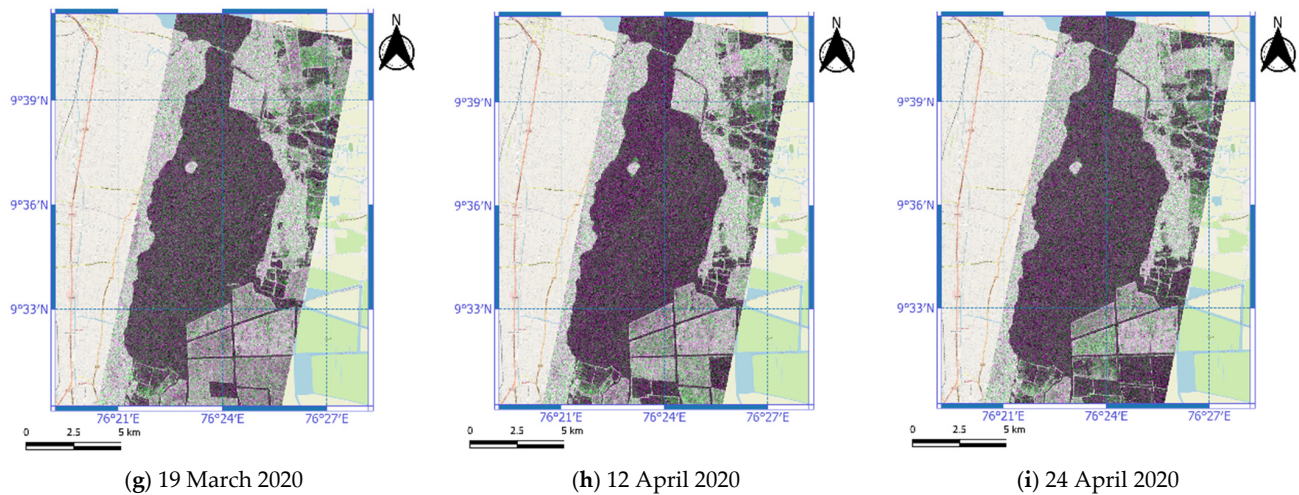


Figure 4. RGB composites (VV, VH, VV/VH) of SAR images acquired over Vembanad Lake, highlighting the temporal changes of water hyacinth within the lake (Sentinel-1, Credits: ESA).

Photographs and local knowledge were used to identify regions of interest (ROIs) where water hyacinth was present. The ROI were included in shapefile (polygons), of clean and infested regions.

Code was then used to analyse the images at the dates where the ground evidence was available. All pixels of VV, VH intensity and their ratio were extracted from within the ROI to provide quantitative comparisons.

An F-Test was used to determine if variance differed between pixel intensity values from clean and infested sites. A *t*-Test was then used to determine if the mean level pixel intensity values differed between the sites. Finally, a single-factor ANOVA was used to further confirm if the different pixel intensities were statistically significant.

Once the detectability was assessed histograms were created using the values from the clean and infested pixel values from within the polygons, the distributions can be seen and are discussed in Figures 5 and 6c. The histograms provided a solution for identifying the optimal threshold to separate infested from clean pixels using single intensity images. The detection maps were obtained by setting a threshold on the intensity of the polarisation channel.

$$\begin{aligned} C_{clean} & \text{ if } I_p < T_p \\ C_{infested} & \text{ if } I_p > T_p \end{aligned} \quad (2)$$

where I_p is the intensity of the polarisation channel and T_p is the threshold obtained by pixel extraction from the ROIs within the lake.

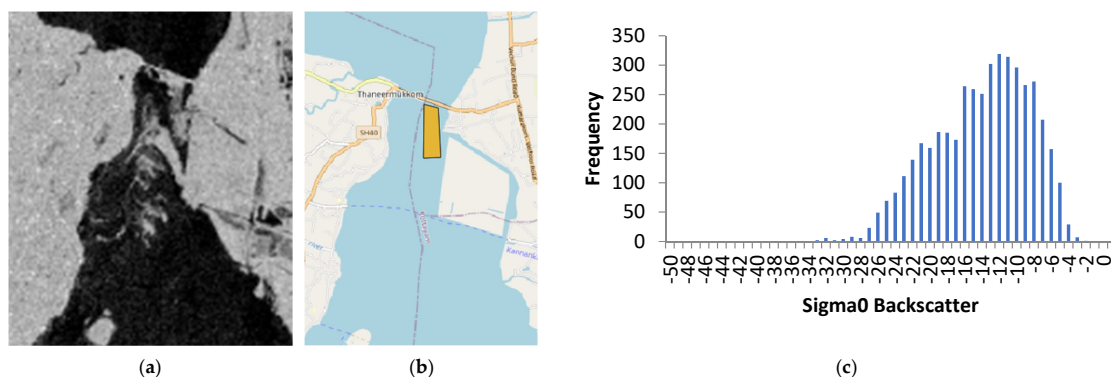


Figure 5. Image from 19 January 2020 in Sentinel-1 VV Channel showing water hyacinth on surface of Vembanad Lake. (a) VV intensity, (b) polygon used for histogram and (c) histogram of pixels in the polygon (Sentinel-1, credits: ESA).

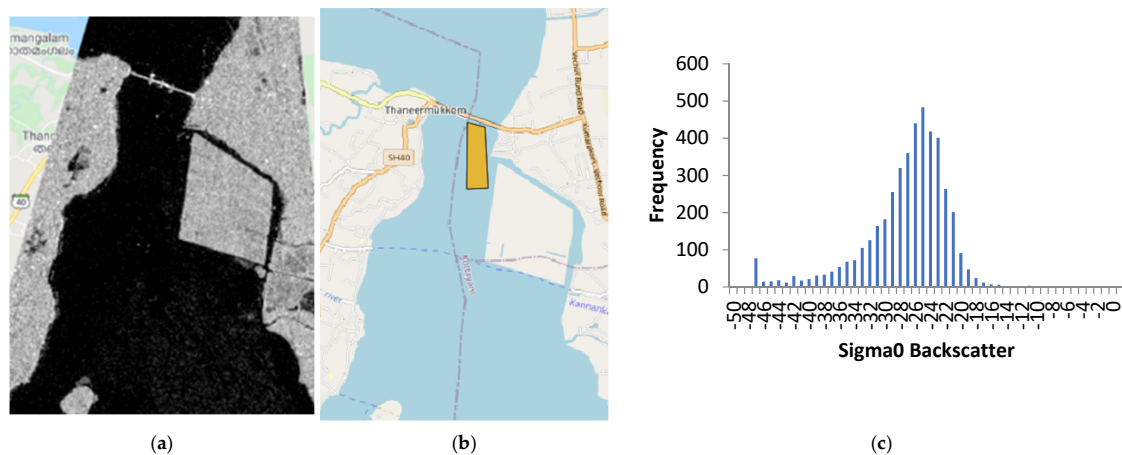


Figure 6. Image from 2 November 2019 in Sentinel-1 V Channel showing reduced water hyacinth on surface of Vembanad Lake. (a) VV intensity, (b) polygon for histogram and (c) histogram of clean water pixels. (Sentinel-1 credits: ESA).

3.7. Change Detection Methods

Sentinel-1 SLC images were processed (Figure 2) in the Sentinel Application Platform (SNAP). These images were calibrated and deburstured before a subset of Vembanad Lake was created and polarimetric matrices were established with a 1×4 multilook used to reduce noise.

Multi-temporal SAR techniques require pixel-to-pixel matching between features within stacked SAR images. Co-registration is the process of layering a number of images in such a way that the same pixels correspond to the same location [47] Co-registration is able to align SAR images, up to fraction of a pixel [48].

Change detectors were used on images of the clean and infested portions. This required us to have two images, a test image and a reference image. To do this, we selected an infested image, with visible water hyacinth, and a clean image where the lake had trace amounts of water hyacinth visible. ROIs were selected so that they encompassed areas of water hyacinth infestation (infested) or areas of clean water (clean). Areas of high-density water hyacinth and low-density hyacinth were selected to evaluate the capabilities of the detectors on differing amounts of infestation.

To benchmark the processing, traditional detectors were used: Difference, Normalised Difference and Ratio Detectors in VV and VH polarisation channels. Additionally, we used newer detectors, Power Difference, Power Ratio [49–51] and the Hotelling–Lowley Trace [52,53] detectors. Once these were implemented, Receiver Operating Characteristic (ROC) curves were displayed to evaluate the performance of each detector. A ROC curve is a graphical technique that plots sensitivity (true detection) against specificity (false alarms) and allows for a visual assessment of a test ability to discriminate between the two [54].

3.8. Standard Change Detectors

Difference: This detector uses changes in radar backscatter intensities by subtracting the intensity values, pixel by pixel, between two separate temporal acquisitions. In the following it is referred to as Diff_XX, where XX represent the polarisation channel (e.g., Diff_HV).

The equation is:

$$\Delta I = |\langle |img_1|^2 \rangle - \langle |img_2|^2 \rangle| > T_1 \quad (3)$$

Normalised Difference: This detector normalises the difference in radar backscatter intensities, allowing for differences in brighter and darker areas to be treated more equally. In the following it is referred to as NDiff_XX.

The equation is:

$$\Delta I_n = \frac{|\langle |img_1|^2 \rangle - \langle |img_2|^2 \rangle|}{\langle |img_1|^2 \rangle + \langle |img_2|^2 \rangle} > T_2 \quad (4)$$

Ratio Detector: This detector divides the intensity values, pixel by pixel, between two separate temporal acquisitions. In the following it is referred to as Ratio_XX.

The equation is:

$$\rho_I = \frac{\langle |img_1|^2 \rangle}{\langle |img_2|^2 \rangle} > T_3 \quad (5)$$

Optimisation of Power Ratio: This detector finds the best linear combination of polarimetric channels, which optimises the contrast between infested and clean portions. The detector finds the best scattering mechanism by diagonalizing an appropriate matrix operator.

The equation is:

$$\rho_c = \frac{\omega^{*T}[T_{11}]\omega}{\omega^{*T}[T_{22}]\omega} = \frac{P_1}{P_2} \quad (6)$$

$$[T_{22}]^{-1}[T_{11}]\omega = \lambda\omega$$

The algorithm was proven to detect changes in forestry and landcover (e.g., bare soil) in the SARTOM data. Within the AGRISAR data, the detector was able to identify changes in more urban and built-up areas [51].

In the following is referred to Pow1 (to indicate the maximum eigenvalue).

Optimisation of Power Difference: This optimises the differences between two covariance matrices by finding the linear combination of polarimetric channels, which provides the highest (or smallest) difference. This detector has primarily been used in an agricultural setting using AGRISAR data [50].

In the following is referred to dif1 (to indicate the maximum eigenvalue). This is because we know water hyacinth is producing an increase in the backscattering.

The equation is:

$$\Delta = \omega^{*T}[T_{22}]\omega - \omega^{*T}[T_{11}]\omega$$

$$\Delta = \omega^{*T}([T_{22}] - [T_{11}])\omega = \omega^{*T}[T_c]\omega \quad (7)$$

$$[T_c]\omega = \lambda\omega$$

Hotelling–Lawley Trace (HLT): This detector evaluates the dissimilarity of two covariance matrices by calculating the trace of the following matrix.

The equation is:

$$int_N = Trace\{T_{22}^{-1}T_{11}\} \quad (8)$$

There is a link between the HLT and the Optimal Ratio, where the trace looks at the means, instead of the maximum of the same searching space [55]. This detector achieved accuracies of 80–95% with error rates of 3–6% on multiple tests [52]. The detector was able to indicate changes in land cover, urban areas and water bodies. ROC curves were used to compare the Hotelling–Lawley Trace (HLT) against the Likelihood Ratio Test (LRT), where it was shown that the proposed change detection method gave detection and error rates comparable to that of the generalised likelihood ratio test [52].

A heatmap of water hyacinth accumulations was then created using the best performing detector.

4. Results

4.1. Initial Observations of Lake Vembanad

The results in this work were validated by ground inspections of Vembanad Lake. Figure 3 shows a picture of the lake where the water hyacinth coverage is clearly visible; it should be noted that, while there is the possibility for other macrophytes to be present within the scene, the infestation was primarily made from water hyacinth.

4.2. Preliminary Analysis of Backscattering

Preliminary inspection of the time-series data showed that there were several dates where the VV intensity over the lake areas peaked and troughed. Figure 4 presents Sentinel-1 RGB composites (VV, VH, VV/VH) for different dates of acquisition. The SAR image is overlaid onto a background google maps showing the surrounding Kuttanad region.

The bright spots seen in Figure 4a–f, are in line with the theory that we increased surface roughness (and therefore brightness) within the SAR image due to more backscatter from a target over the water surface, and these images represent infested dates.

As a comparison, we can also see some examples of the lake without any infestation. Figure 4d,g–i represents images of clean dates, where there is reduced signs of water hyacinth within the lake.

The initial sighting of possible water hyacinth on the lake surface is promising as it is evidence in favour of our hypothesis that water hyacinth will increase the surface roughness of the lake surface and will therefore be visible in SAR imaging. In the following subsections, we validated this using ground measurements.

4.3. Validation and Statistical Analysis

In Figure 5 we can see an image from 19 January 2020 showing the VV channel intensity (Figure 5a). Please note the ground validation was carried out on the 26 of January (one week after) although it was known to the team that water hyacinth was accumulating near the barrage before that date. A polygon was established to cover the area of water hyacinth seen close to the barrage within the lake seen in Figure 5b. This location was selected as it showed clear water hyacinth infestation and could be used for threshold selection. The histogram of the highlighted area is shown in Figure 5c, where we can see that the intensity values of the pixels are negatively skewed (left skewed), shown by the long tail to the left of the peak within the histogram, which is at the higher range of intensity values in the histogram. It appears that the full area does not become the same brightness, which suggests that the signal may be sensitive to the amount of water hyacinth. Testing this will require the challenging collection of samples (to measure biomass) that we could not attempt in this research.

We do not have aerial photos at the time of the sentinel acquisition to produce a better separation inside the histogram.

Figure 6 is used as a comparison showing the VV intensity channel from 2 November 2019, where the infestation of water hyacinth is much lower within the lake. The same shapefile from Figure 6b is used so that a similar number of pixels is collected from the same coordinates within the lake. In Figure 6c we can see that the distribution of pixels looks more like a normal distribution as the peak is more central and there is a more symmetrical distribution. A comparison between Figures 5c and 6c shows that there is a difference in the distribution of clean and infested pixels from these dates. These patterns have also been shown in Akbari et al., 2021 [56].

4.4. Statistical Analysis of Pixels

An F-Test (Table 1) was initially used to compare the variance between clean pixels and infested pixels. The clean pixels were extracted from 2 November 2019 using the shapefile seen in Figure 6b. The infested pixels were extracted from 19 January 2020 using the same shapefile. We used the shape files near the land because we could not produce more accurate shape files for areas far from the land.

Table 1. F-test for clean (2019-11-02) and infested (2020-01-19) pixels.

	Infested Pixels	Clean Pixels
Mean	−14.49377783	−27.60624561
Variance	30.03353544	34.71476606
Observations	5252	5252
Df	5251	5251
F	0.865151601	
P ($F \leq f$) one-tail	7.78587×10^{-8}	
F Critical one-tail	0.937802638	

The test considers the hypotheses:

H_{01} —There is equal variance between clean and infested pixels.

H_{a1} —There is unequal variance between clean and infested pixels.

We can reject the null hypothesis at a 0.1% significance level, proving the variance between clean pixels and infested pixels is significantly different.

Thus, an unpaired *t*-test that does not assume equal variance was used to assess whether the mean backscatter values are similar.

The hypotheses are as follows:

H_{02} —There is no significant difference between the means for clean and infested pixel values.

H_{a2} —There is a significant difference between the means for clean and infested pixel values.

Table 2 shows that the mean of the infested pixels is noticeably higher than the clean pixels. The *t*-statistic of 118.09 is greater than the critical value for a two-tail test. We can also see that the *p*-value calculated is very close to 0; therefore, we can reject the null hypothesis at a 0.1% significance level, proving that the mean levels between the pixel values are significantly different. In fact, a stronger, one-tailed test allows us to conclude that the backscattering values are significantly higher for infested than for clean pixels.

Table 2. Summary of *t*-test results, comparing clean (2019-11-02) and infested (2020-01-19) pixels.

	Infested Pixels	Clean Pixels
Mean	−14.4938	−27.60624561
Variance	30.03354	34.71476606
Observations	5252	5252
Hypothesised Mean Difference	0	
Df	10447	
<i>t</i> Stat	118.0953	
P ($T \leq t$) one-tail	0	
<i>t</i> Critical one-tail	2.326705	
P ($T \leq t$) two-tail	0	
<i>t</i> Critical two-tail	2.5763	

4.5. Threshold on Intensities

The change detection threshold was set using the previous histograms in Figures 5c and 6c, where a threshold of −14 dB was used to separate the infested and clean pixels. This preliminary threshold was set, as no clean pixel had an intensity value greater than −14 in Figure 6c. In Figure 5c, we can see pixel values of −14 dB and higher intensities due to the histograms including infested pixels; therefore, a threshold of −14 dB will highlight pixels of those intensities.

Figure 7 shows the detection mask in blue. The fact that we used a restrictive threshold only allows us to detect areas with clear infestation. We can clearly see the two channels with water flow. The selection of the threshold provides quite different output values.

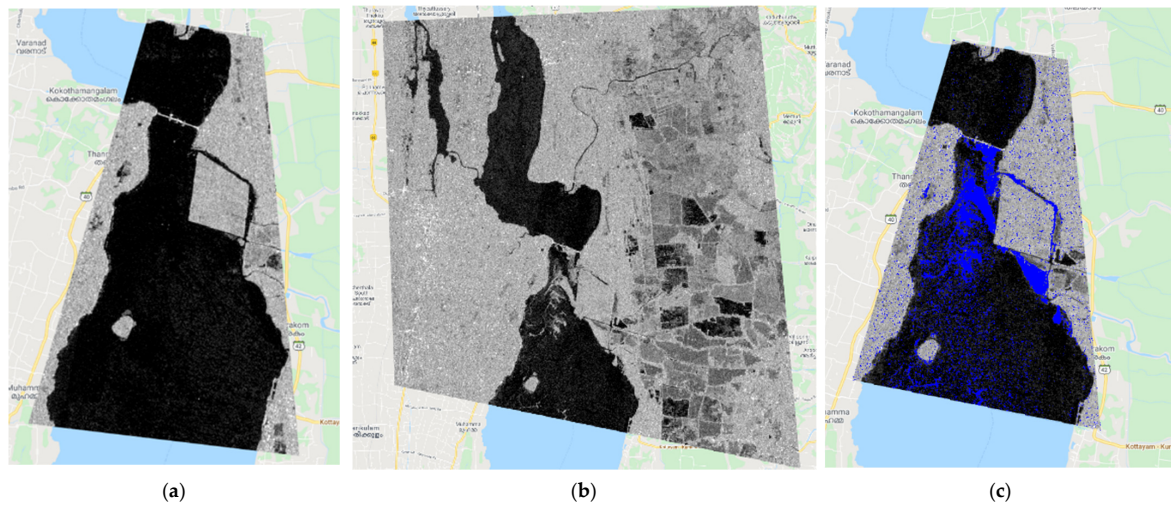


Figure 7. Detection mask using the difference of VV channel intensities. Images compared: (a) 2 November 2019 and (b) 19 January 2020. (c) Detection mask using previous images. (Sentinel-1, credits: ESA).

4.6. Change Detection: January 2020 vs. April 2020: Barrage

Using the Sentinel-1 SLC data, the covariance matrices were used to create masks of clean and infested regions of Vembanad Lake. Two separate, non-overlapping regions were selected for the clean and infested masks. For the 19 January 2020 and 24 April 2020 images, we used the same mask presented in Figure 8.

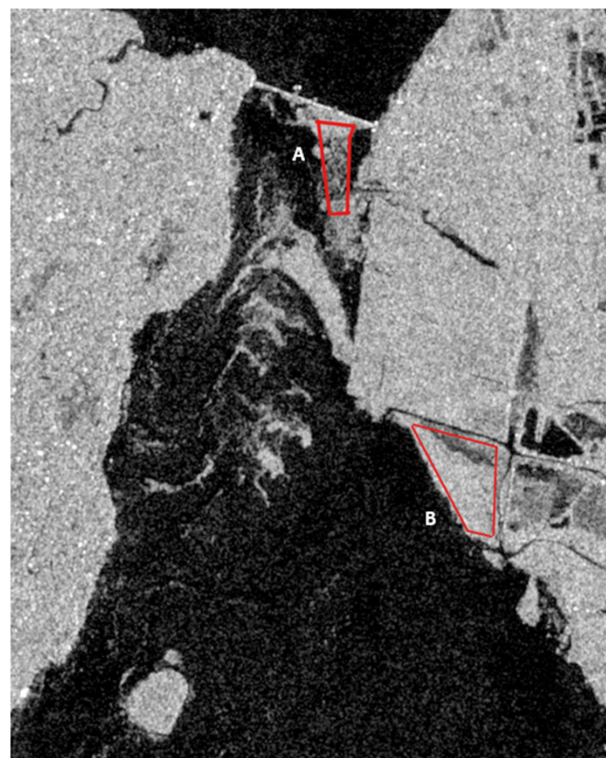


Figure 8. Mask of barrage-infested region within Vembanad Lake, 19 January 2020. (A,B) The red polygons highlight the region used for the infected masks. (Sentinel-1, Credits: ESA).

The water hyacinth infestation was concentrated around the south of barrage and south of the paddy within Vembanad Lake. This infested mask south of the barrage (Figure 8A) was chosen as it was one of the closest Sentinel-1 pass-over dates to the validated date available where the water hyacinth infestation within the lake was visible near the barrage (Figure 3).

For the clean areas, we used the pixels of the 24 April 2020 as shown in Figure 9.

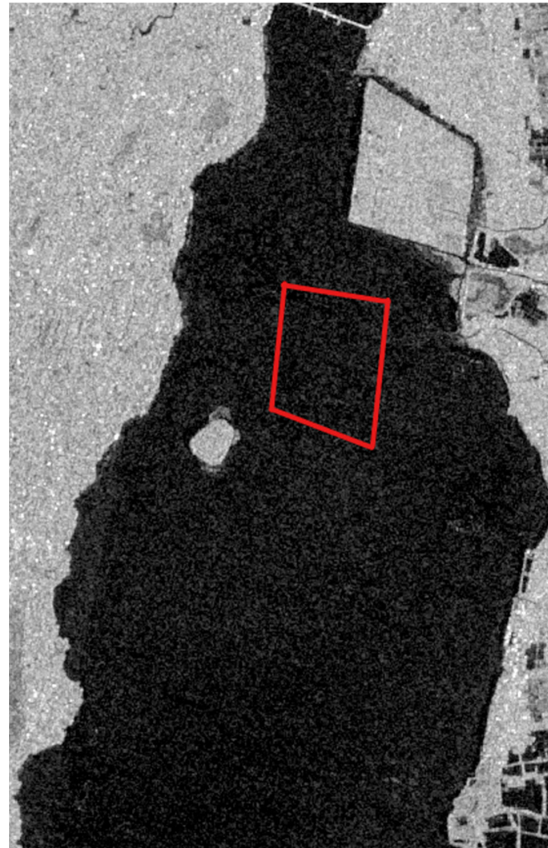


Figure 9. Mask of clean region within Vembanad Lake, 24 April 2020. The red polygon highlights the region used for the clean mask. (Sentinel-1, Credits: ESA).

The Difference, Normalised Difference, Ratio Detectors in VV and VH polarisation channels, as well as the Power Difference, Power Ratio and Trace detectors were implemented across the covariance matrices from 24 April 2020 and 19 January 2020 using the masks for the clean and infested regions within each image.

A ROC curve was then created to assess the accuracy of these detectors showing probability of detection against probability of a false alarm.

Figures 10 and 11 show the ROC curves assessing the ability of the change detectors to classify water hyacinth from 19 January 2020 and 24 April 2020. Figure 11, being in Log10, is more stretched toward the smaller values. On the Y-axis we can see the probability of detection (Pd), or true positive, on the X-axis we can see the probability of false alarm (Pf), or false positive. Pd indicates how many correct positive detections of water hyacinth occurred within the sample masks. Please note that areas may also include some open water regions, underestimating the probability of detection. Pf indicates how many incorrect positive detections occurred within the sample masks. Knowing this, we can see that Figures 10 and 11 show the Power Difference (Dif1), Power Ratio (Pow1) and Trace detector (HLT) as the most accurate detectors out of the algorithms tested, with a true positive detection of around 95% with 0.1% false alarms. We can also see that the ratio_VV, normalised difference_VV and normalised difference_VH detectors perform very poorly with a positive detection of around 20% with 1% false alarms.

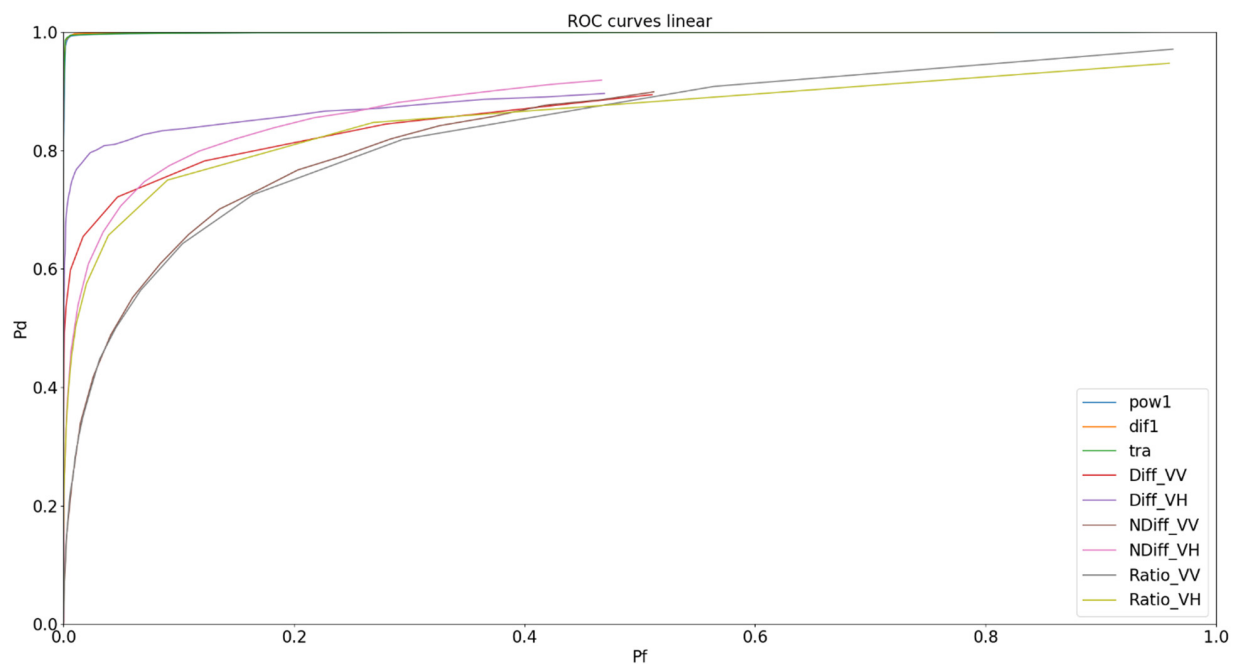


Figure 10. ROC curve in linear format showing change detectors used on 19 January 2020 barrage & 24 April 2020 data: Difference VV and VH (Diff_), Ratio VV and VH (Ratio_), Normalised Difference (NDiff_), Power Difference (Dif1), Power Ratio (Pow1) and Trace (HLT).

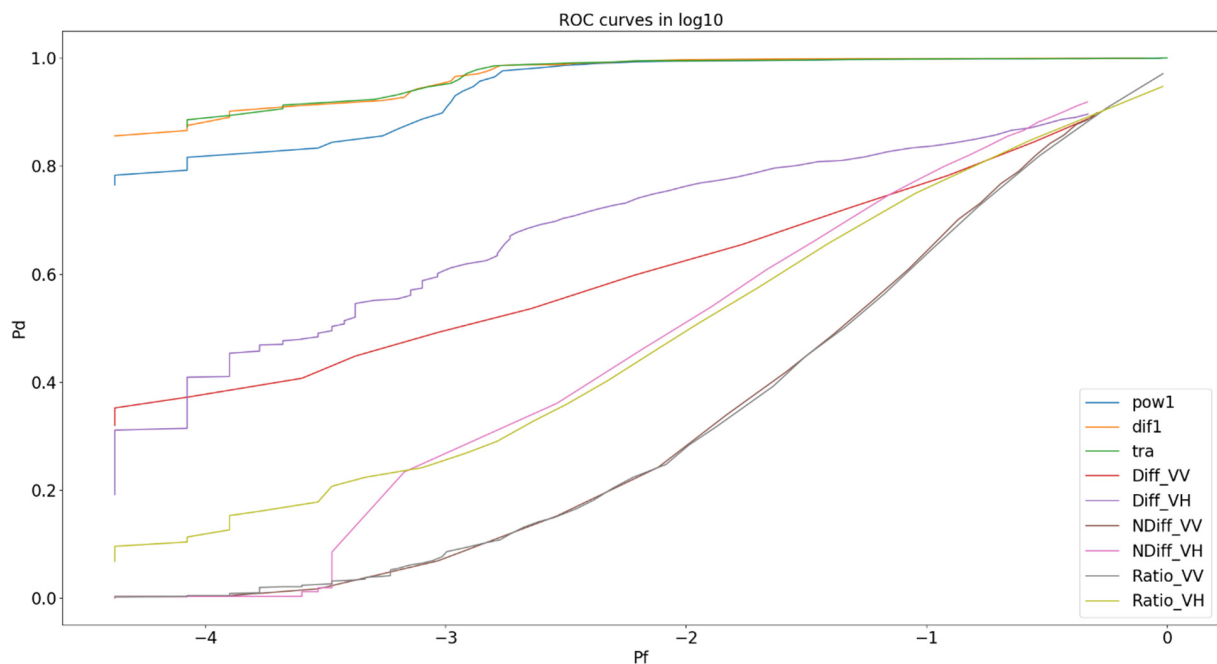


Figure 11. ROC Curve in Log10 showing change detectors used on 19 January 2020 barrage & 24 April 2020 data: Difference VV and VH (Diff_), Ratio VV and VH (Ratio_), Normalised Difference (NDiff_), Power Difference (Dif1), Power Ratio (Pow1) and Trace (HLT).

4.7. Change Detection: January 2020 vs. 24 April 2020: Paddy

The detectors were tested on another infested region from January against the same clean April date (Figure 9) to check the consistency of the results.

The next test involved using an infested mask of the water hyacinth infestation south of the paddy (Figure 8B) within Vembanad Lake on 19 January 2020. As explained previously,

this date was the nearest match to the validated picture taken of water hyacinth infestation in Figure 3.

This location was identified by local researchers as an area prone to being infested by water hyacinth. These researchers also confirmed that the paddy fields in the north get infested and the water hyacinth is moved south to clear the fields for sowing. In this image, we do not have ground pictures directly south of the paddy because the area was hard to reach; however, they corroborate the fact that we can detect water hyacinth with good accuracies.

Figures 12 and 13 show the ROC curves assessing the ability of the change detectors to classify water hyacinth south of the paddy from 19 January 2020 and 24 April 2020. These figures reinforce that the Dif1, Pow1 and HLT detectors are more accurate in when compared to their traditional counterparts. Figures 12 and 13 also show that every detector had higher true positive detections when used on the 19 January paddy field infested data mask (Figure 8B). This is because the block of infesting water hyacinth seems to be more compact without open channels in it. The results here are possibly closer to the actual capability of SAR proving true positive detection probabilities of 98% in the Dif1, Pow1 and HLT detectors, with probability of false alarms being as low as 0.1% for the best detectors. Once again, the ratio_VV and normalised difference_VH detectors performed the poorest out of those tested, with true positive detection probabilities of 50% with 1% probability of false alarms.

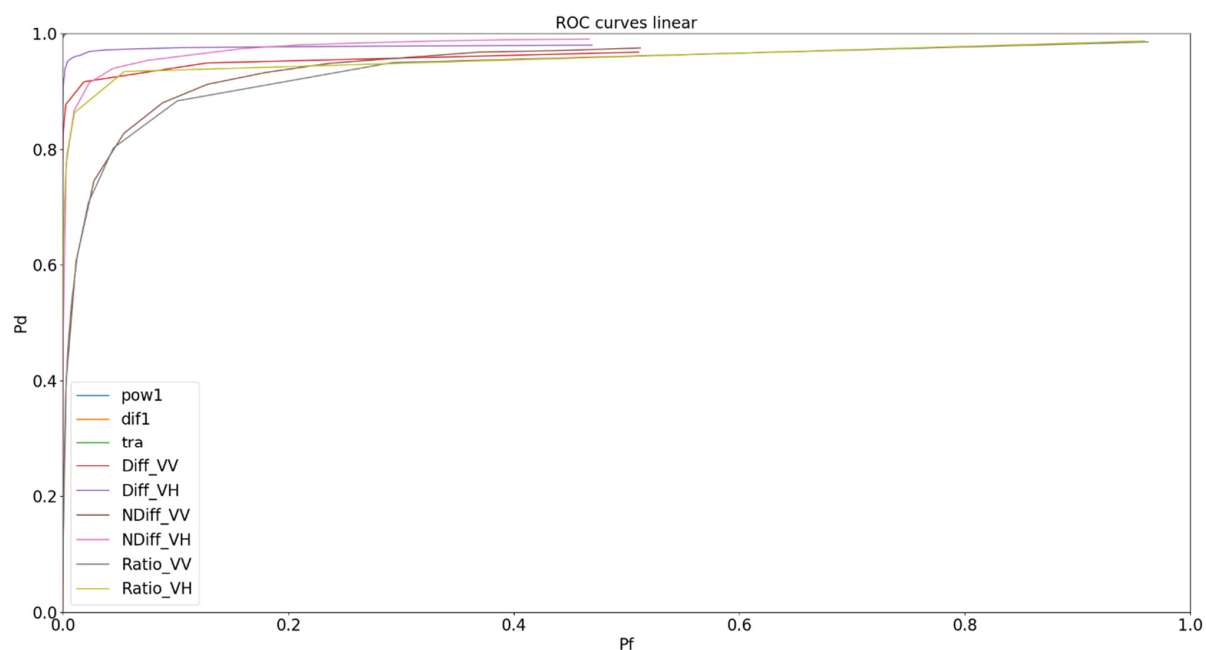


Figure 12. ROC Curve in Log10 showing change detectors used on 19 January 2020 paddy & 24 April 2020 data: Difference VV and VH (Diff_), Ratio VV and VH (Ratio_), Normalised Difference (NDiff_), Power Difference (Dif1), Power Ratio (Pow1) and Trace (HLT).

From visualisation of the images and from the previous pixel value analysis (Tables 1 and 2), it was noticed that the sigma value differed in different pixels within the patches of water hyacinth. This is speculated to be caused by changing densities in water hyacinth.

4.8. Change Detection: October 2019 vs. 24 April 2020: Paddy

A new date of water hyacinth infestation was selected to further test the capabilities of the detectors. An image from 19 October 2019 of sparser water hyacinth infestation south of the paddy within Vembanad Lake was selected (Figure 14). In this image, we do not have ground validation pictures from 19 October 2019; however, the local researchers corroborated further again that this area is prone to water hyacinth build-up.

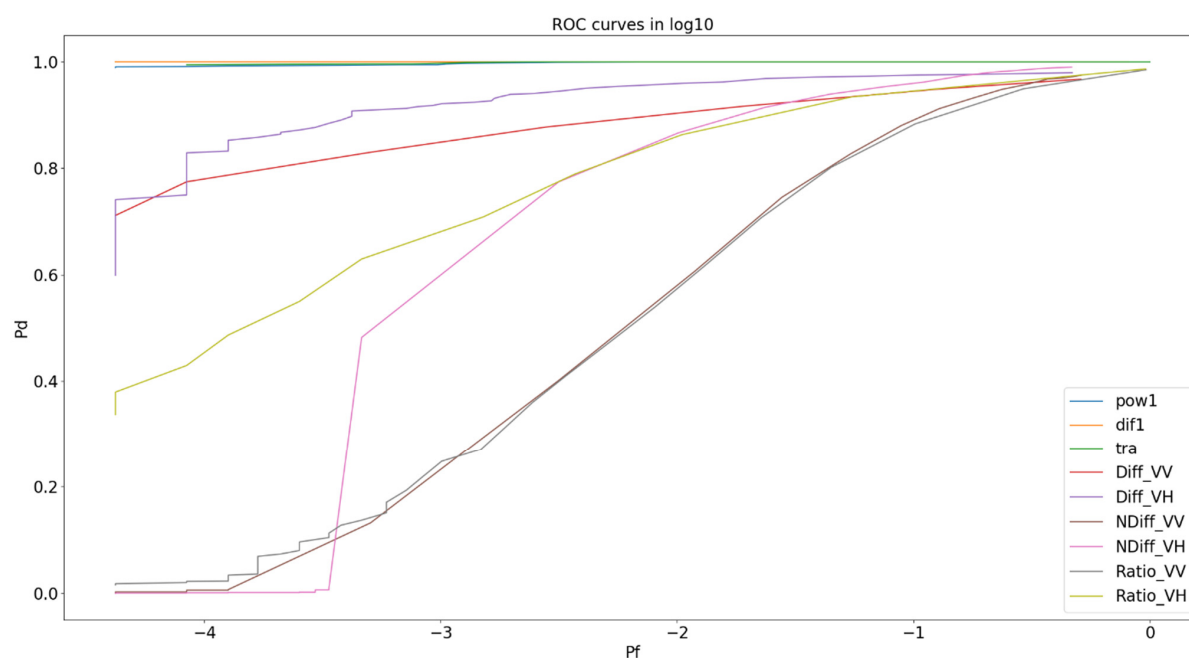


Figure 13. ROC curve in linear format showing change detectors used on 19 January 2020 paddy & 24 April 2020 data: Difference VV and VH (Diff_), Ratio VV and VH (Ratio_), Normalised Difference (NDiff_), Power Difference (Dif1), Power Ratio (Pow1) and Trace (HLT).

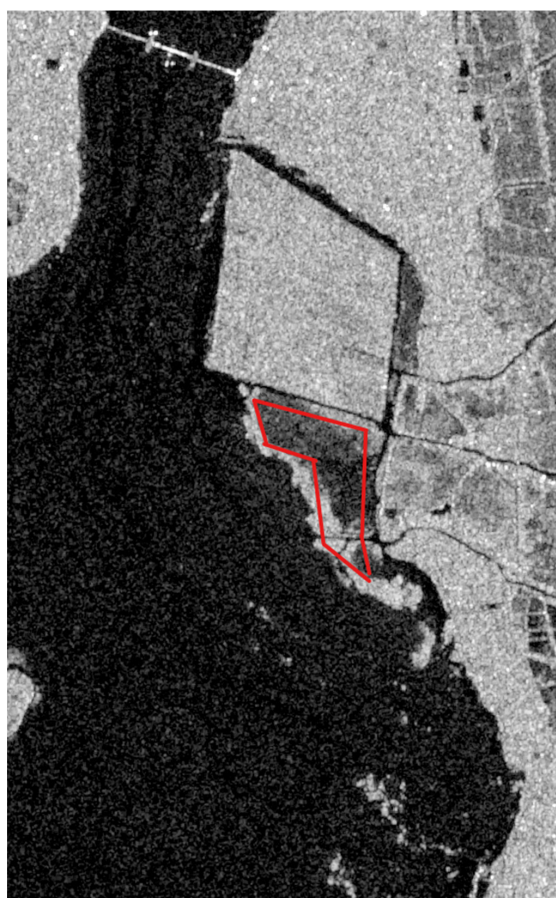


Figure 14. Mask of infested region, south of barrage, within Vembanad Lake, 19 October 2019. The red polygon highlights the region used for the infected mask. (Sentinel-1, Credits: ESA).

This infested mask was tested against the same April clean date (Figure 9). From this new infested mask, ROC curves were created to assess the accuracy of the detectors on the lower-density water hyacinth (Figures 15 and 16).

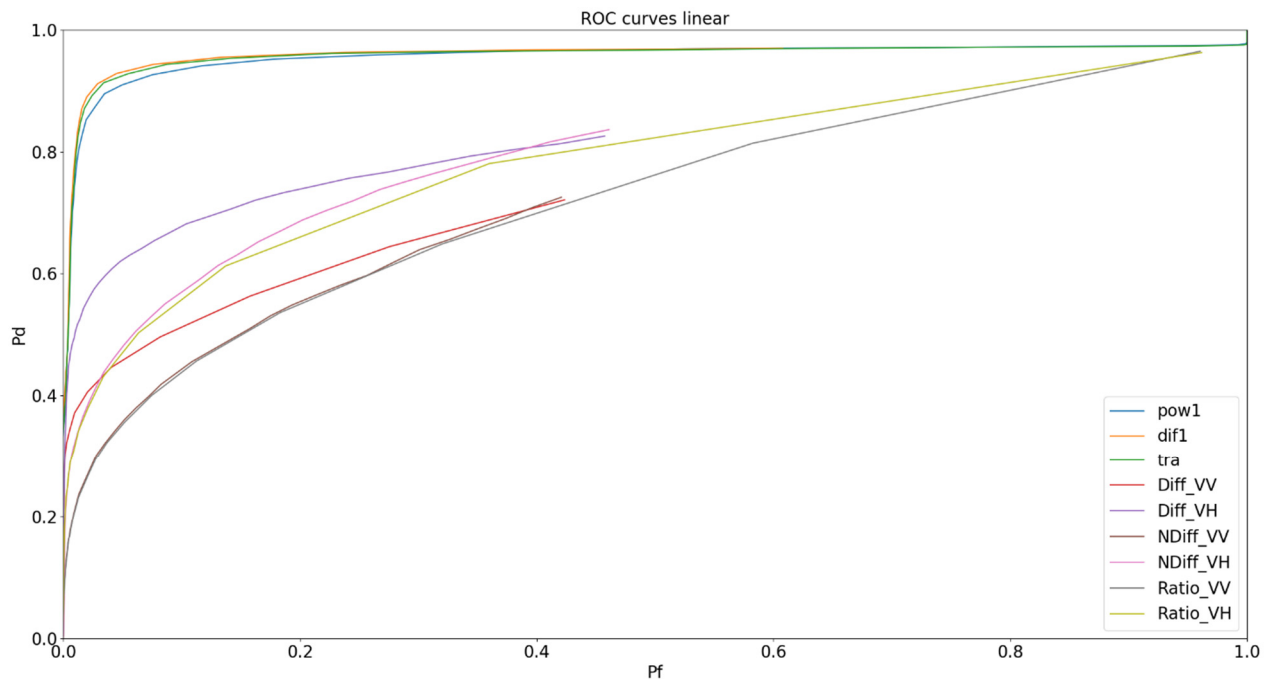


Figure 15. ROC curve in linear format showing change detectors used on 19 October 2019 paddy & 24 April 2020 data: Difference VV and VH (Diff_), Ratio VV and VH (Ratio_), Normalised Difference (NDiff_), Power Difference (Dif1), Power Ratio (Pow1) and Trace (HLT).

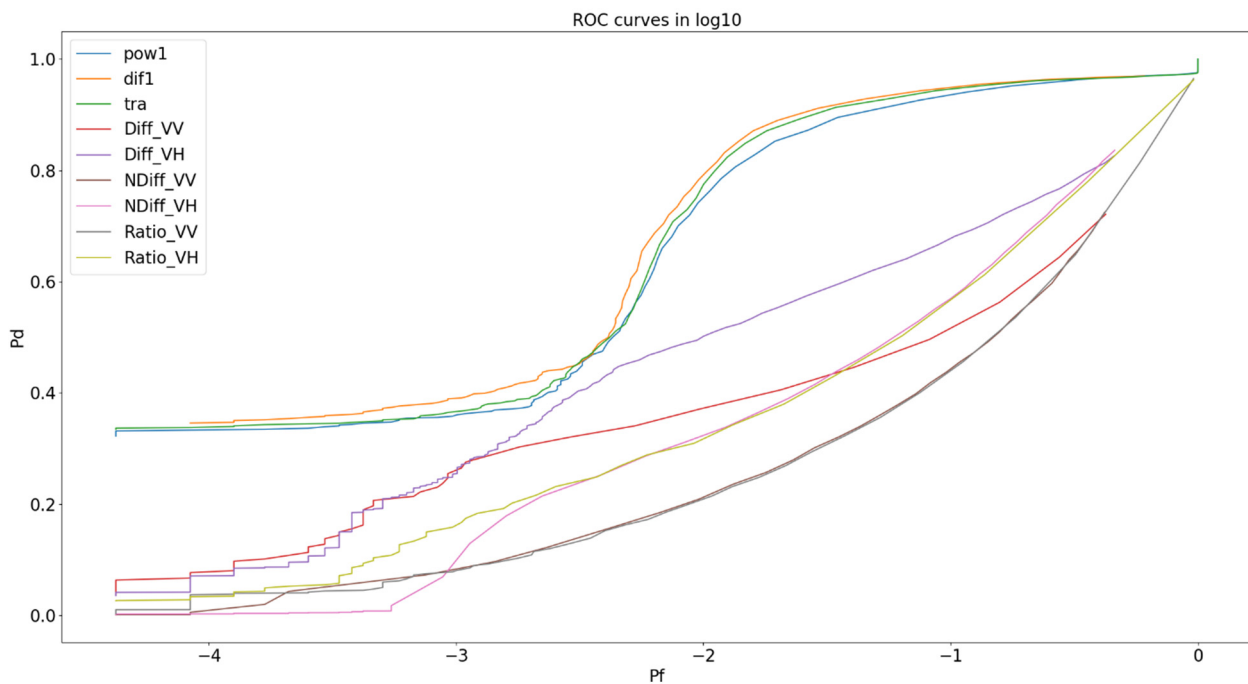


Figure 16. ROC curve in Log10 showing change detectors used on 19 October 2019 paddy & 24 April 2020 data: Difference VV and VH (Diff_), Ratio VV and VH (Ratio_), Normalised Difference (NDiff_), Power Difference (Dif1), Power Ratio (Pow1) and Trace (HLT).

From Figures 15 and 16, it is evident that the change detectors performed significantly better on the areas of high-density water hyacinth. However, the true positive detection of the Pow1, Dif1 and HLT detectors is around 35–40% positive detection with 0.1% false alarms.

4.9. Heatmap of Water Hyacinth Infestation: 12 January 2019–1 January 2021

To understand the patterns of water hyacinth accumulation and travel within Vembanad Lake, a heatmap was created from the 46 SLC acquisitions taken between January 2019 and January 2021. The Optimisation of Power Difference detector was used for the detection of the aquatic weed, as it was one of the best performing detectors from those tested. The 46 SLC acquisitions were all tested with the clean mask region from Figure 9. A heatmap (Figure 17) was then created, where areas of darker yellows/reds signify locations, which were prominent in the detections of water hyacinth.

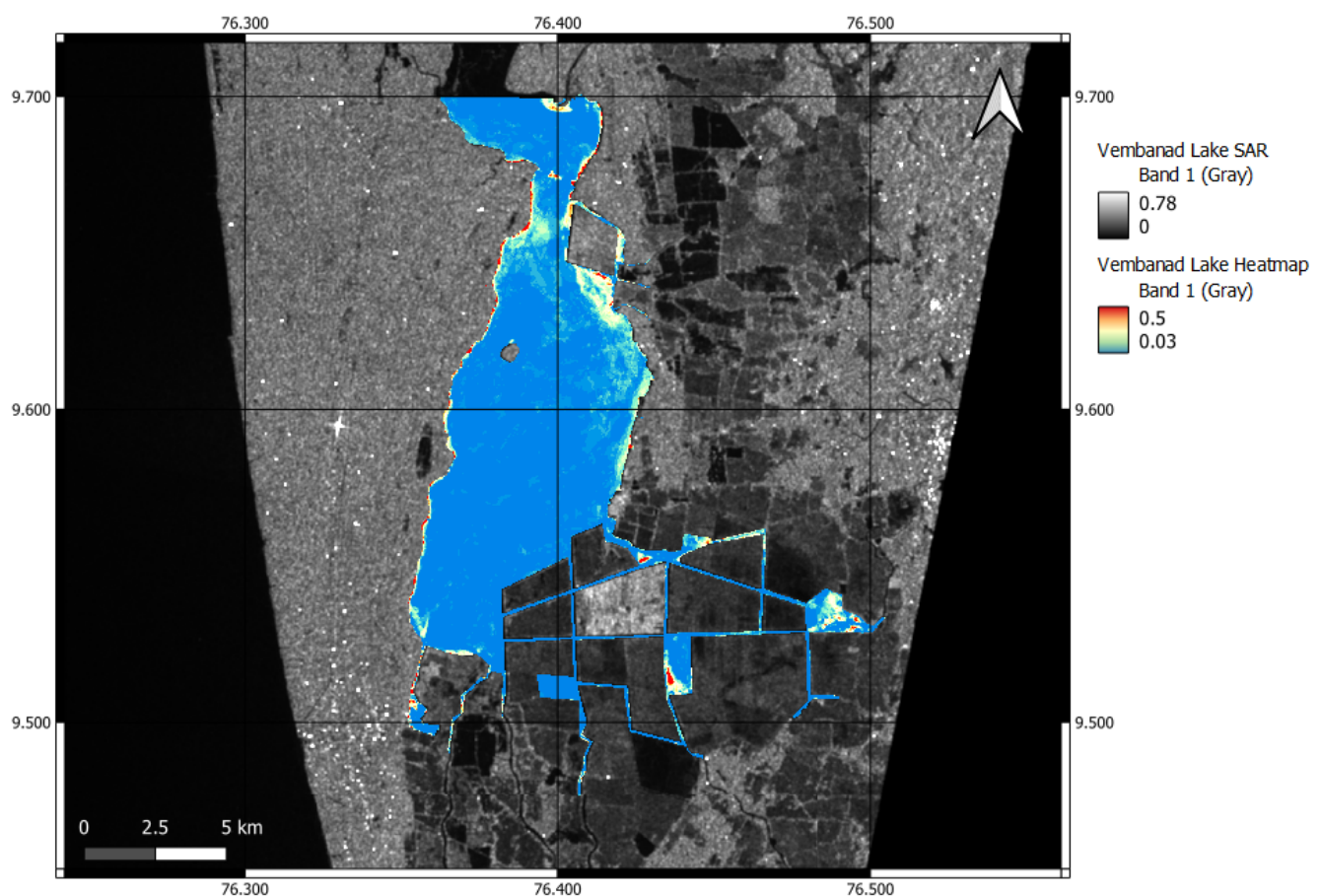


Figure 17. Heatmap of water hyacinth infestations on Vembanad Lake from 12 January 2019 to 1 January 2021 (46 total acquisitions). Background SAR image acquired 12 January 2019 (Sentinel-1, Credits:ESA). Blue = low concentration–Red = high concentration.

Figure 17 shows that there is some significant build-up of water hyacinth within the channels between the southern paddies during the time period from 2019 to 2021. There is also a strong presence of water hyacinth underneath the northern paddy and near the barrage that crosses the lake.

5. Discussion

5.1. Visibility of Water Hyacinth

The first hypothesis was to validate that water hyacinth is visible in SAR imaging. Through the processing of Sentinel-1 SAR data taken from Vembanad Lake, water hyacinth

appears visible in intensity images. The change in surface roughness and backscatter caused by the presence of water hyacinth allows for visibility. Ground validation from the Thanneermukkom Barrage on Vembanad Lake was provided by local researchers, who validated the location of water hyacinth patches in the area. Other examples of water hyacinth infestations were found throughout the data from 2019 to 2021, where the amount of infestation fluctuated throughout this timeline. However, this can be attested to the seasonal dynamics of water hyacinth [57] and regimes implemented to clean the Kochi backwaters, which includes Vembanad Lake [58].

Pixel extraction shown in the histograms of Figure 2 shows a difference in the intensity of pixels within infested areas compared to clean areas. The homogenous infested site has a peak at -12 dB, with a majority of points concentrated around the -16 dB to -6 dB values. We can also see that a majority of pixel values are no higher than an intensity value of -26 dB within the pixels extracted.

Interestingly, the homogenous clean site shows a more normal distribution with a peak at -25 dB with a concentration of pixels around -31 dB to -21 dB.

Tables 1 and 2 show the statistical analysis of the pixel values that were tested between the infested and clean sites. The mean value of infested pixels was -14.5 dB, with clean pixels having a mean value of -27.6 dB, showing that the infested pixels had a higher intensity when compared with the clean site pixels. The F-test, T-test and ANOVA conducted on the clean and infested datasets showed a statistical significance at 0.1%. This proved that the intensity values had a significant difference.

We also learned that different conditions of water hyacinth could be viewed throughout the images, which was seen in differing Sigma values within the water hyacinth pixels. One hypothesis is that these changes in Sigma values are from differing densities of water hyacinth on the lake. Another hypothesis is that these differing Sigma values could potentially be attributed to poor plant quality and therefore lower plant water content, which influences the dielectric constant [59].

5.2. Detectors

Initially, single-intensity image detectors were tested. These traditional algorithms show that even a simple detector can distinguish the presence of water hyacinth within the lake with adequate accuracy. However, more detectors were tested to provide comparisons of accuracy in traditional detectors against more recent powerful detectors.

The ROC curves in Figures 10 and 11 show that the Ratio VV detector and Normalised Difference VV and VH detector performed the worst out of the selection of detectors used, with a large false positive rate for these detectors. It can also be noted that the Difference VH and Difference VV detectors performed the best out of the traditional detectors. The more powerful detectors: Power Difference (Dif1), Power Ratio (Pow1) and Trace detector (HLT), all showed higher true detection rates. This increase in accuracy in the Power Difference/Ratio and Trace detector can be attributed to the more powerful techniques used to create them, as previously described in the Methodology section. Figures 12 and 13 further reinforced this by showing the powerful detectors performing best out of the algorithms used on another separate dataset with true positive detections of $\sim 95\%$.

The ROC curves in Figures 10–13 also further emphasised that all detectors have increased true positive detections on what we believe to be higher-density water hyacinth. The performance on high-density water hyacinth reached $\sim 97\%$ true positive detections with 0.1% false alarms in the powerful detectors. The lower-density water hyacinth testing in Figures 15 and 16 showed a positive detection rating of around 35–40% with 0.1% false alarms in the more powerful detectors. This lower positive detection rating can be attributed to the mixing of differing densities of water hyacinth and the mixing of exposed water and water hyacinth within the infestation. This may be due to the image being taken during the rainy season in India, where the waters will be more disturbed and can disperse the infestation.

Previous studies that use the classification of optical data on aquatic vegetation species have found accuracies of 84.6% [23] and 83% [26], using unsupervised classifications. The detectors used in this study show similar, and greater, accuracies when used on high-density water hyacinth; however, the lower-density accuracies perform poorly when compared with optical counterparts.

The heatmap of Vembanad Lake shows areas that are prone to water hyacinth infestation. We can see locations near the northern paddy and barrage have a tendency for high concentrations of water hyacinth. This can also be seen in the channels to the south of the lake, where more paddies are found. The usage of this heatmap can aid future work within the lake, where targeting of control measures can be focussed in these areas to reduce the impact of the invasive species.

6. Conclusions

While there is an established background for the practice of remote sensing in the detection of aquatic plants, the use of SAR has yet to be fully exploited in the detection of invasive water hyacinth. This study shows that water hyacinth appears visible in SAR imaging and can be monitored through radar remote sensing. The backscattering differences in water hyacinth and clean water provide a basis for change detection algorithms to be implemented and used. Overall, the results indicate that change detection systems using SAR data can identify lower-density water hyacinth within Vembanad Lake, with accuracies varying from 35% to 40%, depending on the constraint on false alarms rate and higher-density water hyacinth with accuracies varying from 90 to 98% depending on the false alarms rate.

However, future research can implement a further range of detectors, such as Wishart [60–62] and a Perturbation Filter [63], to analyse detectors with potentially greater accuracies. Implementing a texture detector can also provide benefits for detection.

The ground validation established that the invasive aquatic vegetation was composed of water hyacinth; however, future work would need to be undertaken to understand the ability to discriminate between water hyacinth with respect to other aquatic vegetation classes.

Further ground validation providing information on water hyacinth density in different areas would provide information on the different conditions seen within SAR imaging. This ground validation could be acquired using drone data. However, coverage of the lake and accurate density measurements may be hard to achieve considering the large area and the difficulties associated with evaluating plant height and density from high-resolution optical images. However, the combination of optical, SAR and in situ monitoring will strengthen the detection of water hyacinth within the lake and will be used in future studies.

Author Contributions: Conceptualization, M.D.S. and A.M.; methodology, M.D.S. and A.M.; validation, G.N.P.; formal analysis, M.D.S., V.A. and A.M.; investigation, M.D.S.; data curation, M.D.S. and V.A. and A.M.; writing—original draft preparation, M.D.S., A.M., V.A. and D.B.; writing—review and editing, All Authors; supervision, A.M. and S.M. All authors have read and agreed to the published version of the manuscript.

Funding: Sentinel-1 data provided courtesy of the European Space Agency Copernicus Programme. This work was supported by the UKRI Global Challenges Research Fund through grant (FF\1920\1\37) from the Royal Academy of Engineering; and the Discovery Element of the European Space Agency's Basic Activities (ESA Contract No. 4000132548/20/NL/MH/hm).

Acknowledgments: Thanks to Cristian Silva, Stirling University, for help with coding some of the algorithms.

Conflicts of Interest: The authors declare no conflict of interest.

References

1. Sriraman, S. Long term perspectives on inland water transport in India. *RITES J.* **2010**, *12*, 18.1–18.14.
2. Sabitha, N.M.; Sreedevi, B.G.; Kumar, V.S. *Recent Advances in Materials, Mechanics and Management*; CRC Press: London, UK, 2019.
3. O'Neil, A. India Distribution of the Workforce Across Economic Sectors from 2010 to 2020. 2021. Available online: <https://www.statista.com/statistics/271329/distribution-of-gross-domestic-product-gdp-across-economic-sectors-in-india/> (accessed on 17 May 2021).
4. Sidhu, B.S.; Kandlikar, M.; Ramankutty, N. *Increasing the Resilience of Indian Agriculture to Intraseasonal Monsoon Variability through Optimised Irrigation Strategies*; American Geophysical Union, Fall Meeting: Washington, DC, USA, 2019.
5. Reddy, M.S.; Char, N.V.V. Management of Lakes in India. *Lakes Reserv.* **2006**, *11*, 227–237. [\[CrossRef\]](#)
6. Guereña, D.; Neufeldt, H.; Berazneva, J.; Duby, S. Water hyacinth control in Lake Victoria: Transforming an ecological catastrophe into economic, social and environmental benefits. *Sustain. Prod. Consum.* **2015**, *3*, 59–69. [\[CrossRef\]](#)
7. Naidu, V.S.G.R.; Deriya, A.; Naik, S.; Paroha, S.; Khankhane, P.J. Water use efficiency and phyto-remediation potential of water hyacinth under elevated CO₂. *Indian J. Weed Sci.* **2014**, *46*, 274–277.
8. Tellez, T.R.; Lopez, E.M.R.; Granado, G.L.; Perez, E.A.; Lopez, R.M.; Guzman, J.M.S. The water hyacinth, *Eichhornia crassipes*: An invasive species in the Guadiana River Basin (Spain). *Aquat. Invasions* **2008**, *3*, 42–53. [\[CrossRef\]](#)
9. Gezie, A.; Assefa, W.W.; Getnet, B.; Anteneh, W.; Dejen, E.; Mereta, S.T. Potential impacts of water hyacinth invasion and management on water quality and human health in Lake Tana watershed, Northwest Ethiopia. *Biol. Invasions* **2018**, *20*, 2517–2534. [\[CrossRef\]](#)
10. Masifwa, W.F.; Twongo, T.; Denny, P. The impact of water hyacinth, *Eichhornia crassipes* (Mart) Solms on the abundance and diversity of aquatic macroinvertebrates along the shores of northern Lake Victoria, Uganda. *Hydrobiologia* **2001**, *452*, 79–88. [\[CrossRef\]](#)
11. Alimi, T.; Akinyemiju, O.A. Effect of water hyacinth on water transportation in Nigeria. *J. Aquat. Plant Manag.* **1991**, *29*, 109–112.
12. Kumari, M.; Syamaprasad, S.; Das, S. Inland waterways as an alternative and sustainable transport in Kuttanad Region of Kerala, India. In *Advances in Water Resources Engineering and Management*; Springer: Singapore, 2020.
13. Mathur, P.; Mathur, S.M. Water Hyacinth: A useful plant to improve rural economy. In *Energy and Environment*; Springer: Singapore, 2018.
14. Center, T.; Hill, M.; Cordo, H.; Julien, M. Water Hyacinth. In *Biological Control of Weeds in the United States*; Agricultural Research Service: Washington, DC, USA, 2002.
15. Fetahi, T. Eutrophication of Ethiopian water bodies: A serious threat to water quality, biodiversity and public health. *Afr. J. Aquat. Sci.* **2019**, *44*, 303–312. [\[CrossRef\]](#)
16. Petterson, D. Water hyacinth: Blessing or curse?—Dams & water storage. *Water Sanit. Afr.* **2019**, *14*, 14–15.
17. Turnipseed, R.K.; Moran, P.J.; Allan, S.A. Behavioral responses of gravid *Culex quinquefasciatus*, *Aedes aegypti*, and *Anopheles quadrimaculatus* mosquitoes to aquatic macrophyte volatiles. *J. Vector Ecol.* **2018**, *43*, 252–260. [\[CrossRef\]](#)
18. Honlah, E.; Segbefia, A.Y.; Appiah, D.O.; Mensah, M.; Atakora, P.O.; Sabater, A. Effects of water hyacinth invasion on the health of the communities, and the education of children along River Tano and Abby-Tano Lagoon in Ghana. *Cogent Soc. Sci.* **2019**, *5*, 1619652. [\[CrossRef\]](#)
19. Datta, A.; Maharaj, S.; Prabhu, G.N.; Bhowmik, D.; Marino, A.; Akbari, V.; Rupavatharam, S.; Sujeetha, J.A.R.P.; Anantrao, G.G.; Poduvattil, V.K.; et al. Monitoring the Spread of Water Hyacinth (*Pontederia crassipes*): Challenges and Future Developments. *Front. Ecol. Evol.* **2021**, *9*. [\[CrossRef\]](#)
20. Neil, C.; Spyrakos, E.; Hunter, P.D.; Tyler, A.N. A Global approach for chlorophyll-a retrieval across optically complex inland waters based on optical water types. *Remote Sens. Environ.* **2019**, *229*, 159–178. [\[CrossRef\]](#)
21. Tyler, A.N.; Hunter, P.D.; Spyrakos, E.; Groom, S.; Constantinescu, A.M.; Kitchen, J. Developments in Earth observation for the assessment and monitoring of inland, transitional, coastal and shelf-sea waters. *Sci. Total Environ.* **2016**, *572*, 1307–1321. [\[CrossRef\]](#)
22. Gholizadeh, M.H.; Melesse, A.M.; Reddi, L. A comprehensive review on water quality parameters estimation using remote sensing techniques. *Sensors* **2016**, *16*, 1298. [\[CrossRef\]](#)
23. Everitt, J.H.; Yang, C.; Escobar, D.E.; Webster, C.F.; Lonard, R.I.; Davis, M.R. Using remote sensing and spatial information technologies to detect and map two aquatic macrophytes. *J. Aquat. Plant Manag.* **1999**, *37*, 71–80.
24. Shilpakar, R.L.; Li, J.X.; Ge, L.; Dawson, P.; Chapman, S. Water hyacinth mapping in Gwydir Wetlands using remote sensing techniques. In Proceedings of the 19th NSW Biennial Weeds Conference Papers, Armidale, Australia, 16–19 October 2017.
25. Dogan, O.K.; Akyurek, Z.; Beklioglu, M. Identification and mapping of submerged plants in a shallow lake using quickbird satellite data. *J. Environ. Manag.* **2009**, *90*, 2138–2143. [\[CrossRef\]](#)
26. Sun, C.; Li, J.; Liu, Y.; Liu, Y.; Liu, R. Plant species classification in salt marshes using phenological parameters derived from Sentinel-2 pixel-differential time-series. *Remote Sens. Environ.* **2021**, *256*, 112320. [\[CrossRef\]](#)
27. Chabot, D.; Bird, D.M. Small unmanned aircraft: Precise and convenient new tools for surveying wetlands. *J. Unmanned Veh. Syst.* **2013**, *1*, 15–24. [\[CrossRef\]](#)
28. Woodget, A.S.; Austrums, R.; Maddock, I.P.; Habit, E. Drones and digital photogrammetry: From classifications to continuums for monitoring river habitat and hydromorphology. *Wires Water* **2017**, *4*, e1222. [\[CrossRef\]](#)
29. Knoth, C.; Klein, B.; Prinz, T.; Kleinebecker, T. Unmanned aerial vehicles as innovative remote sensing platforms for high-resolution infrared imagery to support restoration monitoring in cut-over bogs. *Appl. Veg. Sci.* **2013**, *16*, 509–517. [\[CrossRef\]](#)
30. Aguirre-Gomez, R.; Salmon-Garcia, O.; Gomez-Rodriguez, G.; Peralta-Higuera, A. Use of unmanned aerial vehicles and remote sensors in urban lakes studies in Mexico. *Int. J. Remote Sens.* **2017**, *38*, 2771–2779. [\[CrossRef\]](#)

31. Chabot, D.; Dillon, C.; Shemrock, A.; Weissflog, N.; Sager, E.P.S. An object-based image analysis workflow for monitoring shallow-water aquatic vegetation in multispectral drone imagery. *Int. J. Geo-Inf.* **2018**, *7*, 294. [CrossRef]
32. Lee, G.; Kim, S.; Lee, K. Identification of aquatic plants in the Muncheon Water Reservoir using drone-based information. *J. Environ. Sci. Int.* **2017**, *26*, 685–689. [CrossRef]
33. Gray, P.C.; Ridge, J.T.; Poulin, S.K.; Seymour, A.C.; Schwantes, A.M.; Swenson, J.J.; Johnston, D.W. Integrating drone imagery into high resolution satellite remote sensing assessments of estuarine environments. *Remote Sens.* **2018**, *10*, 1257. [CrossRef]
34. Halls, J.; Costin, K. Submerged and emergent land cover and bathymetric mapping of estuarine habitats using worldview-2 and LiDAR imagery. *Remote Sens.* **2016**, *8*, 718. [CrossRef]
35. Asner, G.P. Cloud Cover in Landsat Observations of the Brazilian Amazon. *Int. J. Remote Sens.* **2001**, *22*, 3855–3862. [CrossRef]
36. De Souza Mendes, F.; Baron, D.; Gerold, G.; Liesenberg, V.; Erasmi, S. Optical and SAR Remote Sensing Synergism for Mapping Vegetation Types in the Endangered Cerrado/Amazon Ecotone of Nova Mutum—Mato Grosso. *Remote Sens.* **2019**, *11*, 1161. [CrossRef]
37. Singh, G.; Reynolds, C.; Byrne, M.; Rosman, B. A remote-sensing method to monitor water, aquatic vegetation, and invasive water hyacinth at national extents. *Remote Sens.* **2020**, *12*, 4021. [CrossRef]
38. Ghoussein, Y.; Nicolas, H.; Haury, J.; Fadel, A.; Pichelin, P.; Hamdan, H.A.; Faour, G. Multitemporal Remote Sensing Based on an FVC Reference Period Using Sentinel-2 for Monitoring *Eichhornia crassipes* on a Mediterranean River. *Remote Sens.* **2019**, *11*, 1856. [CrossRef]
39. Zhang, B.; Perrie, W.; Li, X.; Pichel, W.G. Mapping sea surface oil slicks using RADARSAT-2 quad-polarization SAR image. *Geophys. Res. Lett.* **2011**, *38*. [CrossRef]
40. Brisco, B. Mapping and monitoring surface water and wetlands with Synthetic Aperture Radar. In *Remote Sensing of Wetlands*; CRC Press: Boca Raton, FL, USA, 2015.
41. Hess, L.L.; Melack, J.M.; Affonso, A.G.; Barbosa, C.; Gastil-Buhl, M.; Novo, E.M.L.M. Wetlands of the Lowland Amazon Basin: Extent, vegetative cover and dual-season inundated area as mapped with JERS-1 Synthetic Aperture Radar. *Wetlands* **2015**, *35*, 745–756. [CrossRef]
42. Mohammadimanesh, F.; Salehi, B.; Mahdianpari, M.; Brisco, B.; Motagh, M. Wetland Water Level Monitoring Using Interferometric Synthetic Aperture Radar (InSAR): A Review. *Can. J. Remote Sens.* **2017**, *44*, 247–262. [CrossRef]
43. Lu, Z.; Kwoun, O.-I. Radarsat-1 and ERS InSAR Analysis Over Southeastern Coastal Louisiana: Implications for Mapping Water-Level Changes Beneath Swamp Forests. *IEEE Trans. Geosci. Remote Sens.* **2008**, *46*, 2167–2184. [CrossRef]
44. Silva, T.S.F.; Costa, M.P.F.; Melack, J.M.; Novo, E.M.L.M. Remote sensing of aquatic vegetation: Theory and applications. *Environ. Monit. Assess.* **2008**, *140*, 131–145. [CrossRef]
45. Graciani, S.D.; Novo, E.M.L.M. Determinação da cobertura de macrófitas aquáticas em reservatórios tropicais. In *Anais do XI Simpósio Brasileiro de Sensoriamento Remoto*; SBSR: Belo Horizonte, Brazil, 2003; pp. 2509–2516.
46. Cavalli, R.M.; Laneve, G.; Fusilli, L.; Pignatti, S.; Santini, F. Remote sensing water observation for supporting Lake Victoria weed management. *J. Environ. Manag.* **2009**, *90*, 2199–2211. [CrossRef]
47. Constantini, M.; Zavagli, M.; Martin, J.; Medina, A.; Barghini, A.; Naya, J.; Hernando, C.; Macina, F.; Ruiz, I.; Nicolas, E.; et al. Automatic Coregistration of SAR and optical images exploiting complementary geometry and mutual information. In *Proceedings of the IGARSS 2018—2018 IEEE International Geoscience and Remote Sensing Symposium*, Valencia, Spain, 22–27 July 2018.
48. Li, Z.; Bethel, J. Image Coregistration in SAR Interferometry. *Int. Arch. Photogramm. Remote Sens. Spat. Inf. Sci.* **2008**, *37*, 433–438.
49. Novak, L.M.; Sechtin, M.B.; Cardullo, M.J. Studies of Target Detection Algorithms that use Polarimetric Radar Data. *IEEE Trans. Aerosp. Electron. Syst.* **1989**, *25*, 150–165. [CrossRef]
50. Marino, A.; Alonso-Gonzalez, A. Optimisations for Different Change Models with Polarimetric SAR. In *Proceedings of the EUSAR 2018, 12th European Conference on Synthetic Aperture Radar*, Aachen, Germany, 4–7 June 2018.
51. Marino, A.; Hajnsek, I. A Change Detector Based on an Optimisation with Polarimetric SAR Imagery. *IEEE Trans. Geosci. Remote Sens.* **2013**, *52*, 4781–4798. [CrossRef]
52. Akbari, V.; Anfinsen, S.N.; Doulgeris, A.P.; Eltoft, T.; Moser, G.; Serpico, S.B. Polarimetric SAR Change Detection with the Complex Hotelling-Lawley Trace Statistic. *IEEE Trans. Geosci. Remote Sens.* **2016**, *54*, 3953–3966. [CrossRef]
53. Ghanbari, M.; Akbari, V. Unsupervised Change Detection in Polarimetric SAR Data with the Hotelling-Lawley Trace Statistic and Minimum-Error Thresholding. *IEEE J. Sel. Top. Appl. Earth Obs. Remote Sens.* **2018**, *11*, 4551–4562. [CrossRef]
54. Akobeng, A. Understanding diagnostic tests 3: Receiver operating characters curves. *Acta Paediatr.* **2007**, *96*, 644–647. [CrossRef]
55. Marino, A. Trace coherence: A new operator for polarimetric and interferometric SAR IMAGES. *IEEE Trans. Geosci. Remote Sens.* **2017**, *55*, 2326–2339. [CrossRef]
56. Akbari, V.; Simpson, M.; Maharaj, S.; Marino, A.; Bhowmik, D.; Prabhu, G.N.; Rupavatharam, S.; Datta, A.; Kleczkowski, A.; Sujeetha, J.A.R.P. Monitoring Aquatic Weeds in Indian Wetlands Using Multitemporal Remote Sensing Data with Machine Learning Techniques. In *Proceedings of the 2021 IEEE International Geoscience and Remote Sensing Symposium IGARSS*, Brussels, Belgium, 11–16 July 2021; pp. 6847–6850. [CrossRef]
57. Thamaga, K.H.; Dube, T. Understanding seasonal dynamics of invasive water hyacinth (*Eichhornia crassipes*) in the Greater Letaba river system using Sentinel-2 satellite data. *GIScience Remote Sens.* **2019**, *56*, 1355–1377. [CrossRef]
58. Giri, G.G. KMRL to come up with plan to clean Vembanad Lake. The Times of India. 2017. Available online: <https://timesofindia.indiatimes.com/city/kochi/kmrl-to-come-up-with-plan-to-clean-vembanad-lake/articleshow/61136950.cms> (accessed on 11 July 2020).

-
59. McNairn, H.; Champagne, C.; Shang, J.; Holmstrom, D.; Reichert, G. Integration of optical and Synthetic Aperture Radar (SAR) imagery for delivering operational annual crop inventories. *ISPRS J. Photogramm. Remote Sens.* **2009**, *64*, 434–449. [[CrossRef](#)]
 60. Lee, J.S.; Grunes, M.R.; Kwok, R. Classification of multi-look polarimetric SAR imagery based on complex Wishart distribution. *Int. J. Remote Sens.* **1994**, *15*, 2299–2311. [[CrossRef](#)]
 61. Conradsen, K.; Nielsen, A.A.; Schou, J.; Skriver, H. A test statistic in the complex Wishart distribution and its application to change detection in polarimetric SAR data. *IEEE Trans. Geosci. Remote Sens.* **2003**, *41*, 4–19. [[CrossRef](#)]
 62. Akbari, V.; Anfinson, S.N.; Doulgeris, A.P.; Eltoft, T. A change detector for polarimetric SAR data based on the relaxed Wishart distribution. In Proceedings of the 2015 IEEE International Geoscience and Remote Sensing Symposium, Milan, Italy, 26–31 July 2015.
 63. Marino, A. A Notch Filter for Ship Detection with Polarimetric SAR Data. *IEEE J. Sel. Top. Appl. Earth Obs. Remote Sens.* **2013**, *6*, 1219–1232. [[CrossRef](#)]